

ACCURACY ASSESSMENT OF LINEAR SPECTRAL MIXTURE MODEL(LSMM) IN ESTIMATING VEGETATION ABUNDANCE IN MOUNTAIN AREA

WANG Tianxing¹,CHEN Songlin¹,MA Ya²

(1 College of Geographical Sciences ,Fujian Normal University , Fuzhou 350007 ,China;
2 Guangzhou Institute of Geochemistry, Chinese Academy of Sciences Guangzhou 510640,China)

KEYWORDS: Linear Spectral Mixture Model—LSMM; Terrain Undulation; Correction; Vegetation Abundance; NDVI; MVI; Regression Analysis

ABSTRACT:

Linear Spectral Mixture Model—LSMM which is prevailing presently is one of pixel unmixing models,the unmixing-accuracy of which is restricted by kinds of factors,but now the research about LSMM is mostly focused on appraisalment of linear hypothesis relating to itself and techniques used to select endmembers, nevertheless, the environment conditions of study area which could sway the unmixing-accuracy such as atmosphere reflectance or scatteration and terrain undulation are not studied.This paper probes emphatically into the accuracy uncertainty of LSMM resulting from the terrain undulation with reference to unmixing vegetation abundance under LSMM. ASTER data set was chosen and the C terrain correction was applied to it. Based on this, vegetation abundances were extracted from both pre-C corrected and post-C terrain illumination corrected ASTER using LSMM, then the regression analysis between vegetation abundance and vegetation indices(NDVI and MVI) was further conducted to assess the unmixing accuracy which quantitatively measure the impact of terrain illumination on LSMM. The results indicate that terrain undulation could dramatically constrain the application of LSMM in inversion of vegetation abundance. A improved unmixing accuracy of 17.6% and 18.6% for R2 was achieved in regression against to NDVI and MVI respectively because of the removing terrain undulation by C correction method. Especially, effective removal or minimization of terrain effects is essential in mountainous areas. This study can also provide new theory basis for LSMM applications in mountainous areas. Though we took vegetation abundance as a case study, it should be envisioned that the similar result for other endmember types (water, barren soil, impervious area and so on) could be achieve because of the same impact mechanism of terrain undulation and the identical unmixing procedure with LSMM.

1. INTRODUCTION

Information of land surface targets observed by remote sensing is measured spatially by pixels. Because of the the heterogeneity of ground features and relatively coarse spatial resolution of the satellite borne imagery characterized by TM,ETM+,MODIS,NOAA/AVHRR and so on., it is common that mixture spectra are generated when the pixel is occupied by more than one land-cover class (Ichoku & Karnieli, 1996). The effective information interpreted from mixture pixels is limit for quantitatively analyzing the characteristics of the targets. So a large number of sub-pixel models are developed, such as Linear or non-linear Spectral Mixture Model, Probabilistic model, Geometric-optical

2. TEST SITE AND DATA

Considering the computational burden and representation, we choose the rectangle-shaped suburb area of Fuzhou(26° 10' N, 116 ° 21 ' E at center) where the land covers are abundant(Fig.1). The site is covered by cropland, water, forest vegetation which is dominant, urban cover which mostly locate at SW of the site and bare soils. The terrain condition within the area is relatively undulate with elevation from 50m to 1000m, it is appropriate to investigate the impact of terrain undulation on LSMM.

As one of the recent developments in remote sensing technology , Advanced Spaceborne Thermal Emission and Reflection Radiometer (ASTER) provide substantial improvements over the traditional multispectral sensor, such as Landsat thematic mapper (TM), in spatial, spectral and radiometric resolutions, and has become a vital data source for earth science researchers (Fang Qiu et al,2006). ASTER is a multispectral scanner that produces images of high spatial resolution launched on July, 1999 aboard on the first platform of NASA's Earth Observing System –Terra. The instrument has three bands in the visible and near-infrared (VNIR) spectral range (0.5-0.9 μm) with 15-m spatial resolution, six bands in the shortwave infrared (SWIR) spectral range (1.6-2.4 μm) with 30-m spatial resolution, and five bands in the thermal-infrared (TIR) spectral range (8-12 μm), with 90-m resolution (Kahle et al.,1991;Abrams,2000). An additional backward-viewing telescope with a single band duplicating VNIR band 3 could provide the capability for same-orbit stereogram metric data at 15m spatial resolution.

Another appealing aspect of ASTER data is the open availability of its data and even the on-demand standard products for research use are at very low cost (Rowan & Mars, 2003).

With the advantage of ASTER data described above, we collected ASTER data in Fuzhou area attempting to make use of the improved spatial and spectral information of ASTER data.

WANG Tianxing, E-mail: watixi@163.com. TEL:13459194134.

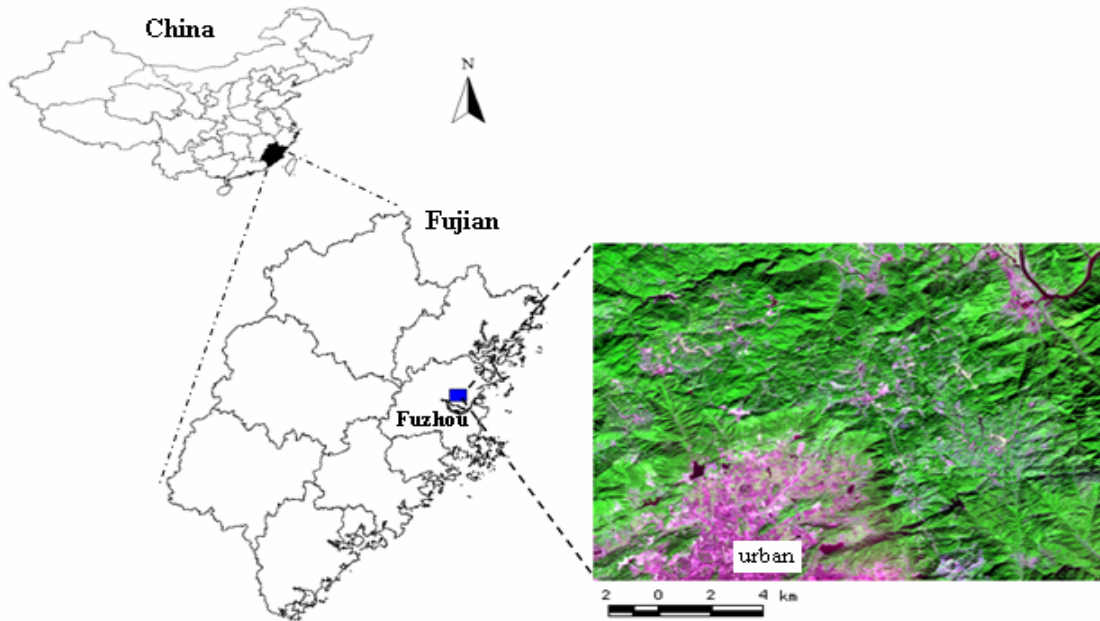


Figure 1 Position of test site

3. METHODS

3.1 Data processing

The ASTER data used in this study are cloud free level 1B data acquired on November 24, 2001. The image has been pre-georeferenced to UTM Zone 50 North projection with WGS-84 datum. The L1B data are in HDF format which contain 15 bands image data, radiance conversion coefficient and ancillary data (Fujisada, 1998), when the data were imported into the ENVI processing system, the conversion coefficient was automatically applied and simultaneously the digital numbers of ASTER were calibrated to radiance. Only the first 9 bands in VNIR and SWIR of ASTER were selected for subsequent analysis because the 5 TIR bands were not relevant to the reflectance of land surface objects. A Fast Line-of-sight Atmospheric Analysis of Spectral Hypercubes- FLASSH based radiometric correction was applied for the first 9 bands. Furthermore, The bands processed above were then stacked into one file and resampled to 15*15 m pixel size using nearest neighbor algorithm. Finally a 1280*750-pixel image was clipped from ASTER data as test site.

To eliminate the terrain undulation, A 1:10000 digital elevation model (DEM) covering study area was collected and then the aspect image and slope image were calculated from the DEM with ArcGIS platform.

3.2 C Terrain undulation correction

Optical imagery is usually affected by variations in brightness due to terrain. The terrain illumination are very common in the satellite imagery captured on undulating earth surfaces, and it could lead to that the same objects display totally different spectral radiance or contrarily different objects exhibit the similar spectral value. Specially an object lying in shadow receives less reflectance than the same object on the sunny side (Klaus I. Itten & Peter Meyer, 1993). In a word, the same targets therefore despite their equal reflectance display varying

spectral radiances due to the topographic undulation under the same sun position. During the selection procedure of endmembers in LSMM, terrain undulation could pose ambiguity, and even lead to false selection or omission, accordingly further sway the unmixing result.

Terrain illumination could be corrected by several methods, but previous literature shows that C-correction is the most effective illumination correction algorithm. (Teillet et al., 1982; Meyer et al., 1993). C-correction is therefore chosen for terrain illumination correction of ASTER data in our study. The basic C-correction formula used as follows:

$$\cos(i) = \cos(s) \cdot \cos(z) + \sin(s) \cdot \sin(z) \cdot \cos(\beta - \beta') \quad (1)$$

$$L_T = a + b \cdot \cos(i), \quad c = a / b \quad (2)$$

$$L_H = L_T \cdot \frac{\cos(z) + c}{\cos(i) + c} \quad (3)$$

Where, $\cos(i)$: cosine of sun's incidence angle for pixel i ;

L_T : radiance observed for sloped terrain (before C-correction);

L_H : radiance observed for horizontal surface (after C-correction);

a, b: intercept and slope of the linear regression line;

s: slope for pixel i ;

z: zenith of sun on image collecting time;

β : azimuth of sun on image collecting time;

β' : aspect for pixel i ;

For the ASTER scene used in our study (collected on 11/24/2001) the sun information checked from ASTER HDF head file was as follows:

Sun elevation:40.902706(complementary angle of zenith)
Sun azimuth: 161.336042

With the sun information listed above, combining the aspect and slope calculated from DEM (section 3.1),the C-correction was applied to ASTER data with 9 bands processed in section 3.1.

The images before and after C-correction were showed in Fig.2. furthermore, the spectral profiles along a random line across mountain area in the before and after C-correction ASTER image were also given in Fig.3.(two random lines shared the same location and distribution).

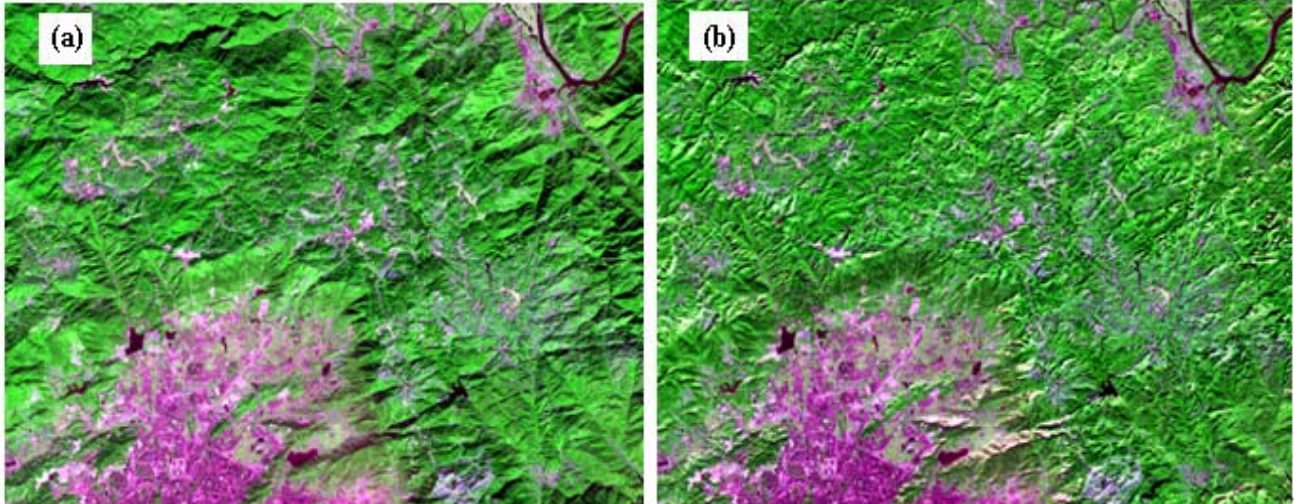


Figure 2 ASTER images of pre-C corrected (a) and post-C corrected (b) (bands132 for RGB)

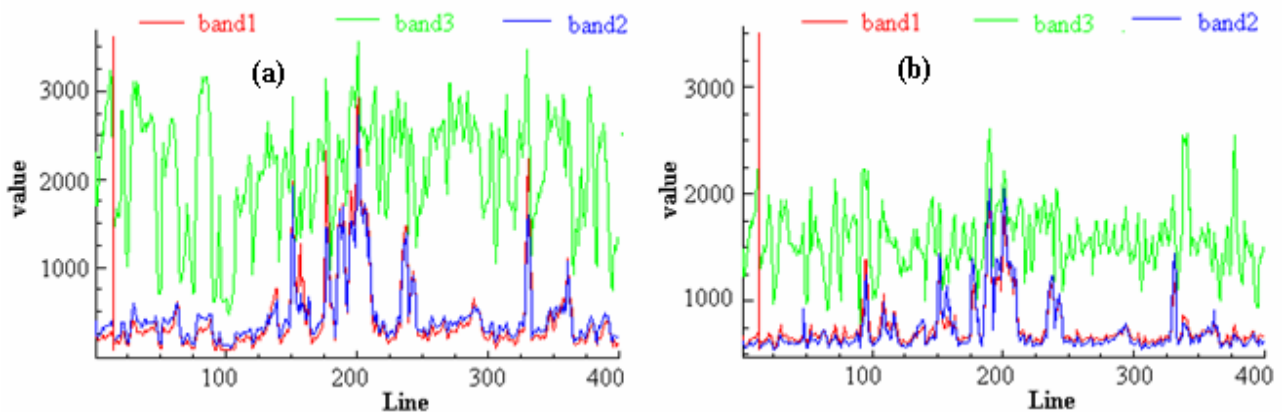


Figure 3 Spectral profiles along a random line across mountain area in the pre-C (a) and post-C (b)corrected ASTER image (two random lines shared the same location and distribution).

3.3 Linear spectral mixture model

When using LSMM, the spectra signals of a pixel are expressed linear combination of finite number of endmembers weighted by their abundances. According to the restriction on abundances, a number of approaches have been developed to analyze LSMM(Ichoku & Karnieli, 1996), such as unconstrained method, augmented matrix method, sum-to-one constrained method and full constrained method(Xin Miao et al,2006), where the augmented matrix method and the sum-to one constrained method confine the sums of endmember abundances to be one or close to one (Smith et al., 1990), and he fully constrained method further requires the endmember abundances to be positive (Brown et al., 1999, 2000;

GarciaHaro et al., 1996; Settle&Drake, 1993;Shimabukuro & Smith, 1991), here we chose the fully constrained LSMM, and the basic algorithms for a pixel were as follows:

$$L_{i\lambda} = \sum_{k=1}^n f_{ki}R_{k\lambda} + \varepsilon_{i\lambda} \quad \text{subject to}$$

$$\sum_{k=1}^n f_{ki} = 1 \quad \text{and} \quad f_{ki} \geq 0 \quad (4)$$

$$RMS = \left[\sum_{i=1}^{\lambda} (\varepsilon_{i\lambda})^2 / n \right]^{1/2} \quad (5)$$

where, $L_{i\lambda}$: reflectance or radiance for pixel i in band λ ;

f_{ki} : abundance of endmember k for pixel i ;

$R_{k\lambda}$: reflectance or radiance value of endmember k in band λ ;

$\varepsilon_{i\lambda}$: residual of pixel i in band λ ;

n : the number of Endmembers in the image, which is less than the number of bands plus one;

RMS: root mean square error for pixel i .

Linear Spectral Mixture Model includes two sequential processing steps: Endmembers selection and linear spectral unmixing . The first step is very important and pivotal. Before solving a spectral mixture model, endmembers with unique spectral signatures need to be identified(Xin Miao et al,2006). Image endmembers have an advantage over library endmembers because they are collected under nearly the same conditions and it is the most common method to collect endmember spectra(Plaza et al, 2004). In addition ,the existence of possible vertical scaling anomalies in ASTER data and SWIR crosstalk from band 5 and band 9 makes the data difficult to use for spectral analysis based on direct comparisons with library or field spectra (Fang Qiu et al,2006;NASA ASTER,2004). Therefore, image endmembers were used in this research.

Previous literatures(Li,2004; Van der Meer & De Jong,2000) demonstrated that the spectral correlations between endmembers could negatively affect the abundance estimates and to enlarge the separabilities between endmember spectra was essential for unmixing successfully. Wu (2004) discussed in his research that significant brightness variation witch could blur the separation of object spectra existed in the spectra of endmember, and simultaneously, proposed a normalization method to remove or reduced the spectra variance while maintaining the useful information to separate the endmembers .To magnify the separabilities between the endmember spectra, normalization approach was applied to pre-C corrected and post-C corrected ASTER data as follows:

$$\bar{L}_b = \frac{L_b}{\frac{1}{n} \sum_{b=1}^n L_b} \quad (6)$$

Where, L_b is the original reflectance or radiance for band b in a pixel; \bar{L}_b is the normalized reflectance or radiance for band b in a pixel; n is the total number of bands (9 for ASTER imagery in this study).

To effectively extract endmembers from relative high dimensional ASTER data and to reduce subsequent computational requirement, a minimum noise fraction (MNF) transform was introduced into to reduce the dimensionality and

to segregate the noise in the original and terrain corrected ASTER data. The MNF transform is composed of two consecutive standard principle component transforms(PC) producing the result data that were not correlated and were arranged in terms of decreasing information content with increasing MNF band number (Green et al,1988; Research Systems, Inc., 2002). Because the information content in the higher-order MNF eigenimages from 1 to 7 in both original and C corrected ASTER imagery was over 95%, consequently, seven ASTER MNF eigenimages was retained for subsequent data processing .

Unlike training site during classification of multispectral data, which takes the mean spectral value of the site as the spectrum of corresponding class, identifying endmember pixels whose spectra are extreme is a complex procedure which usually is equipped with rigorous mathematical algorithms. Especially it is much more difficulty in relative coarse resolution imagery due to the existence of a number of mixture pixels. To determine automatically the pure endmembers, the algorithm namely Pixel Purity Index(PPI) was applied to the MNF eigenimages(generated from pre-C corrected and post-C corrected ASTER) respectively chosen from above procedure. By repeatedly projecting n -dimensional scatter plots of the MNF images onto a random unit vector, two PPI images were formed in which the digital number of each pixel corresponded to the total number of times that the pixel was judged as spectrally pure in all projections. Typically, the brighter the pixel in the PPI image the higher the relative purity because it was more frequently recorded as being a spectrally extreme pixel(Boardman, 1993; Boardman et al., 1995). To reduce the number of pixels to be analyzed for endmember determination and to facilitate the separation of purer materials from mixed pixels(Fang Qiu et al,2006), a iteration number of 10000 and a threshold factor of 2.5 is adopted to the MNF images to select the most pure PPI pixels.

To further refine the selection of the most spectrally pure endmembers from the derived two-dimensional PPI image and more importantly, to label them with specific endmember types, it is essential to reexamine visually the selected pixels in the n -dimensional feature space and to assign them manually to appropriate types(Boardman, 1993; Boardman and Kruse, 1994). So two or more MNF eigenimages were selected to form a n -dimensional scatter plot. All the pixels that were previously selected using the PPI threshold procedure are displayed as pixel clouds in the n -dimensional spectral space. With interactive rotation and visualization in the spectral space, the convex corners of the pixel clouds can be located and designated as the purest spectral endmembers. In our study any combination of bands were selected and the mean spectra of endmember which was represented one type were extracted. Finally, five major types of endmembers were determined from pre-C corrected ASTER imagery and labeled with different types including vegetation, water, impervious area, bare soil and shadow, similarly four endmembers from post-C corrected ASTER imagery and named vegetation, water, impervious area, and bare soil , the spectra of the endmembers extracted from two ASTER data sets were displayed in Fig.4.

With the endmembers collected previously full constrained least square LSMM was applied to pre-C corrected and post-C corrected ASTER data and the vegetation abundance images labeling F1 and F2 were derived.

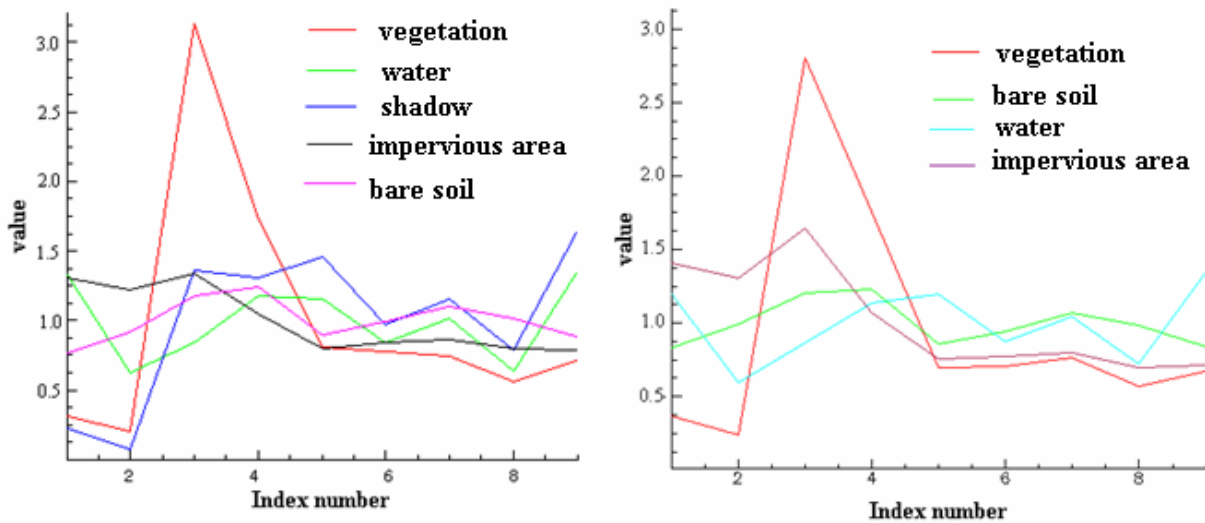


Figure 4 Normalized spectral profile of endmembers extracted from pre-C corrected(left) and post-C corrected (right)ASTER imagery in test site.

4. RESULTS AND DISCUSSION

4.1 Comparison analysis

In mountain area, the terrain undulation effect which could cause shadow or occlusion is not ignored, shadows frequently occur in airborne or space-borne imagery in terrain area with steep slope when the sun elevation angle is low. A number of technologies were developed to circumvent the terrain illumination effect, here we selected the C correction method, Fig2 shows the pre-corrected and post-corrected ASTER images (bands 132 for RGB) of test site. To visually compare the two images same histogram stretch was applied to them and the histogram of C corrected image was matched to the pre-corrected one. As can be seen from Fig2, Fig2(a) had a lot of shadows, the terrain undulation and stereo was apparent across the scene(except the urban area), whereas Fig2(b) which was C corrected had less shadow and the terrain undulation was also inconspicuous. Fig2(b) was even more smooth than Fig2(a), therefore it showed that the terrain undulation impact in study site could be dramatically reduced by C method employed above.

The spectra profile along a random line(Fig3) across undulate area within test site showed that the spectrum variance of objects which were similar in spectra value but locate in both sunny side and opposite side due to the terrain undulation was diminished(Fig3(b)). So the C correction could also effectively reduce the phenomenon characterized by that same targets display varying spectral radiance due to the topographic undulation.

4.2 Regression and validation the C method

LSMM was applied to both pre-corrected and post-corrected ASTER data of study site and two vegetation abundance images were calculated. Unfortunately we did not collect the in situ vegetation abundance data when the ASTER image was acquired. But literatures showed that the vegetation abundance

and normalized difference vegetation index-NDVI or modified vegetation index-MVI have close correlation(Carlson et al,1997;Qi et al,2000;Zeng et al,2000 McDaniel and Haas,1982), the correlation coefficient could indicate the unmixing precision at a certain extent. In addition, our main objective is to investigate the impact on LSMM due to the topographic undulation while not to specifically evaluate the precision for unmixing the vegetation abundance, so the correlation regression method is alternatively feasible for characterizing the negative effect of terrain undulation in this study.

Normalized difference vegetation index and modified vegetation index(MVI) or transformed vegetation index(TVI) maps were derived from pre-corrected ASTER image as follows:

$$NDVI = \frac{R_{NIR} - R_{red}}{R_{NIR} + R_{red}} \quad (7)$$

$$MVI(TVI) = \sqrt{\frac{R_{NIR} - R_{red}}{R_{NIR} + R_{red} + 0.5}} \quad (8)$$

Where R_{NIR} and R_{red} are the spectral reflectances in ASTER near-infrared(band 4) and red(band 3)bands;

To apply regression analysis 5,000 sample points were selected randomly in four images including NDVI, MVI, vegetation abundances from pre-C corrected and pos-C corrected ASTER images. Sequentially the multi-regression analysis between vegetation abundances and vegetation indexes(NDVI and MVI) was employed and the results were displayed in Fig5.

Correlation coefficient (R) or square-R as a indicator index was chosen to quantitate the unmixing precision indirectly. It should be noted that a high R^2 value could indicate the good unmixing precision and also the effectiveness of C correction. As is shown in Fig5 the R^2 between vegetation abundances and vegetation indexes followed by C correction is higher than that of pre-corrected ones. The unmixing precision was improved 17.6% and 18.6% in R^2 value for NDVI and MVI by minimizing or even removing terrain undulation effect using C correction method. On one hand, it proved that, the terrain

undulation could dramatically bias the reflectances of targets and further seriously attenuate the unmixing result for LSMM, and on the other hand, it also validate the effectiveness of C correction method on removing terrain undulation effect again.

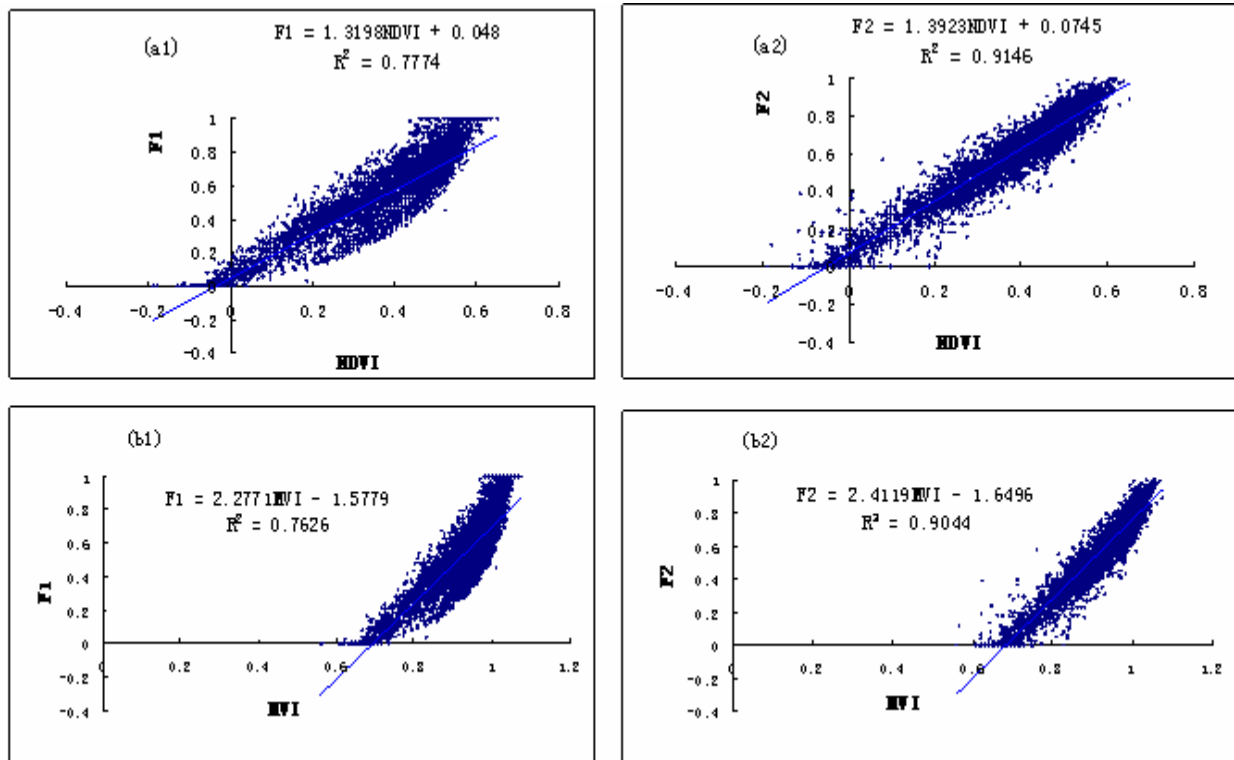


Figure 5 (a1),(a2) Relationships between vegetation abundances and NDVI for pre-C corrected and post-C corrected ASTER imagery. (b1),(b2) Relationships between vegetation abundances and MVI for pre-C corrected and post-C corrected ASTER imagery.

5. SUMMARIES AND CONCLUSIONS

This paper has investigated the impact of terrain undulation on LSMM with reference to unmixing vegetation abundances using LSMM. C correction was used to remove or minimize terrain effects of the original ASTER data and the result showed that the C method was reasonable and effective. The endmember selection procedures such as minimum noise fraction (MNF), pixel purity index (PPI) and n-dimensional visualization were implemented respectively to pre-corrected and post-corrected ASTER data to determine the endmembers effectively. A full constrained least square LSMM was applied to the two data sets and the vegetation abundance images were sequentially derived. Multi-regression analysis between vegetation abundance and vegetation indexes which was employed to validate and estimate the terrain undulation impact on LSMM indicated that terrain undulation could constrain the application of LSMM, typically the unmixing precision was improved 17.6% and 18.6% in R² value for NDVI and MVI by minimizing or even removing terrain undulation effect using C correction method in our study. So specially effective removal or minimization of terrain impact was essential for LSMM applications in moderate or small-scale mountainous areas. The results not only proved the terrain undulation could dramatically bias the reflectances of targets and further seriously attenuate the unmixing result for LSMM but also validate the effectiveness of C correction method on removing terrain undulation impact again.

Though we took vegetation abundance as a case study, it should be envisioned that the similar result for other endmember types (water, barren soil, impervious area and so on) could be achieved because of the same impact mechanism of terrain undulation and the identical unmixing procedure with LSMM. However further studies of different area, different types of imagery and other endmembers are recommended with purpose to inspect the validation and applicability of our results and conclusions. In addition, to acquire specific unmixing precision the accurate and quantitative ground data should be collected. In fact, the atmospheric scattering and scales of the imagery can also behave negative impact on LSMM, to quantitatively evaluate the impacts is our further work in the future.

ACKNOWLEDGEMENTS

the authors like to extend our appreciations to College of Geographical Sciences, Fujian Normal University, Fujian provincial department of science & technology for their foundation support. We also want to gratefully acknowledge all the anonymous reviewer for reviewing the manuscript.

REFERENCES

Adams, J. B., Sabol, D. E., Kapos, V., Almeida, R., Roberts, D. A., Smith, M.O., et al. (1995). Classification of multispectral images based on fractions of endmembers—Application to

- land-cover change in the Brazilian Amazon. *Remote Sensing of Environment*, 52(2), 137–154.
- Abrams, M. (2000). The Advanced Spaceborne Thermal Emission and Reflection Radiometer (ASTER): Data products for the high spatial resolution imager on NASA's Terra platform. *International Journal of Remote Sensing*, 21, 847–859.
- Brown, M., Lewis, H. G., & Gunn, S. R. (2000). Linear spectral mixture models and support vector machines for remote sensing. *IEEE Transactions on Geoscience and Remote Sensing*, 38(5), 2346–2360.
- Boardman, J.W., 1989. Inversion of imaging spectrometry data using singular value decomposition. In: *IGARSS' 89, 12th Canadian Symposium on Remote Sensing*, pp. 2069 – 2072.
- Boardman, J.W., 1993. Automating spectral unmixing of AVIRIS data using convex geometry concepts. In: *Summaries of the 4th Annual JPL Air-borne Geoscience Workshop*, Pasadena, pp. 11 – 14.
- Borel, C. C., & Gerstl, S. A. W. (1994). Nonlinear spectral mixing models for vegetative and soil surfaces. *Remote Sensing of Environment*, 47(3), 403–416.
- Boardman, J.W., Kruse, F.A., Green, R.O., 1995. Mapping target signatures via partial unmixing of AVIRIS data. In: *Summaries, Fifth JPL Airborne Earth Science Workshop*, pp. 23 – 26.
- Boardman, J.W., Kruse, F.A., 1994. Automatic spectral analysis: a geological example using AVIRIS data, North Grapevine Mountain, Nevada. In: *10th Thematic Conference on Geologic Remote Sensing*, Ann Arbor, pp. 407 – 418. Boardman, J.W., Kruse, F.
- Brown, M., Gunn, S. R., & Lewis, H. G. (1999). Support vector machines for optimal classification and spectral unmixing. *Ecological Modelling*, 120(2 – 3), 167–179.
- Charles Lchoku, Arnon Karnieli. A Review of Mixture Modeling Techniques for Sub-Pixel Land Cover Estimation. *Remote Sensing Rewiews*, 1996, 13(1): 161~186
- Chabrillat, S., Pinet, P.C., Ceuleneer, G., Johnson, P.E., Mustard, J.F., 2000. Ronda peridotite massif: methodology for its geological mapping and lithological discrimination from airborne hyperspectral data. *International Journal of Remote Sensing*, 21, 2363–2388.
- Carlson T N, Ripley D A. On the relation between NDVI, fractional vegetation cover, and leaf area index. *Remote Sensing of Environment*, 1997, 62 (3): 241-252.
- Dengsheng Lu, Qihao Weng. (2006) Spectral mixture analysis of ASTER images for examining the relationship between urban thermal features and biophysical descriptors in Indianapolis, Indiana, USA. *Remote Sensing of Environment*, 104, 157 – 167.
- Fang Qiu, Mohamed Abdelsalam, Pathik Thakkar. (2006) Spectral analysis of ASTER data covering part of the Neoproterozoic Allaqi-Heiani suture, Southern Egypt. *Journal of African Earth Sciences*, 44, 169-180.
- Fujisada, H. (1998). ASTER level-1 data processing algorithm. *IEEE Transactions on Geoscience and Remote Sensing*, 36, 1101–1112.
- Gong, P., Miller, J. R., & Spanner, M. (1994). Forest canopy closure from classification and spectral unmixing of scene components—Multisensor evaluation of an open canopy. *IEEE Transactions on Geoscience and Remote Sensing*, 32(5), 1067–1080.
- Green, A.A., Berman, M., Switzer, P., Craig, M.D., 1988. A transformation for ordering multispectral data in terms of image quality with implications for noise removal. *IEEE Transactions on Geoscience and Remote Sensing* 26, 65 – 74.
- GarciaHaro, F. J., Gilabert, M. A., & Melia, J. (1996). Linear spectral mixture modelling to estimate vegetation amount from optical spectral data. *International Journal of Remote Sensing*, 17(17), 3373–3400.
- Ichoku, C., & Karnieli, A. (1996). A review of mixture modeling techniques for sub-pixel land cover estimation. *Remote Sensing Reviews*, 13, 161–186.
- Ichoku, C., & Karnieli, A. (1996). A review of mixture modeling techniques for sub-pixel land cover estimation. *Remote Sensing Reviews*, 13, 161–186.
- Ju, J. C., Kolaczyk, E. D., & Gopal, S. (2003). Gaussian mixture discriminant analysis and sub-pixel land cover characterization in remote sensing. *Remote Sensing of Environment*, 84(4), 550–560.
- Keshava, N., & Mustard, J. F. (2002). Spectral unmixing. *IEEE Signal Processing Magazine*, 19(1), 44–57.
- Kahle, A. B., Palluconi, F. D., Hook, S. J., Realmuto, V. J., and Bothwell, G. (1991). The Advanced Spaceborne Thermal Emission and Reflectance Radiometer (ASTER). *Int. J. Imaging Systems Tech.* 3, 144-156.
- Klaus I. Itten, Peter Meyer. (1993). Geometric and Radiometric Correction of TM Data of Mountainous Forested Areas, *IEEE Transactions on Geoscience and Remote Sensing*, 31(4): 764-770.
- Li, J. (2004). Wavelet-based feature extraction for improved endmember abundance estimation in linear unmixing of hyperspectral signals. *IEEE Transactions on Geoscience and Remote Sensing*, 42(3), 644–649.
- McDaniel K C, Haas R H. Assessing mesquite-grass vegetation condition from Landsat. *Photogrammetric Engineering and Remote Sensing*, 1982 (48): 441–450.
- Meyer, P., Itten, K.I., Kellenberger, T., Sandmeier, S. and Sandmeier, R., 1993. Radiometric Corrections of Topographically Induced Effects on Landsat TM Data in an Alpine Environment, *ISPRS Journal of Photogrammetry and Remote Sensing*, 48, 17-28.
- Neville, R. A., Levesque, J., Stenz, K., Nadeau, C., Hauff, P., & Borstad, G. A. (2003). Spectral unmixing of hyperspectral imagery for mineral exploration: Comparison of results from SFSI and AVIRIS. *Canadian Journal of Remote Sensing*, 29(1), 99–110.

- NASA ASTER, 2004. Advanced Spaceborne Thermal Emission and Reflection Radiometer. Available from: <<http://asterweb.jpl.nasa.gov>>.
- Peterson, S. H., & Stow, D. A. (2003). Using multiple image endmember spectral mixture analysis to study chaparral regrowth in southern California. *International Journal of Remote Sensing*, 24(22), 4481–4504.
- Patrick Hostert, Achim Röder, Joachim Hill.(2003). Coupling spectral unmixing and trend analysis for monitoring of long-term vegetation dynamics in Mediterranean rangelands. *Remote Sensing of Environment* ,87,183–197.
- Pu, R., Xu, B., & Gong, P. (2003). Oakwood crown closure estimation by unmixing Landsat TM data. *International Journal of Remote Sensing*, 24(22), 4433–4445.
- Plaza, A., Martinez, P., Perez, R., & Plaza, J. (2004). A quantitative and comparative analysis of endmember extraction algorithms from hyperspectral data. *IEEE Transactions on Geoscience and Remote Sensing*, 42(3),650–663.
- Quarmby, N. A., Townshend, J. R. G., Settle, J. J., White, K. H., Milnes, M., Hindle, T. L., et al. (1992). Linear mixture modeling applied to AVHRR data for crop area estimation. *International Journal of Remote Sensing*, 13(3),415–425.
- Qi J, Marsett R C, Moran M. S., Goodrich D. C, P. Heilman, Y. H. Kerr, G. Dedieu, A. Chehbouni and X. X. Zhang. Spatial and temporal dynamics of vegetation in the San Pedro River basin area. *Agricultural and Forest Meteorology* ,2000(105): 55-68.
- Rowan, L.C., Mars, J.C., 2003. Lithologic mapping in the Mountain Pass, California area using Advanced Spaceborne Thermal Emission and Reflection Radiometer (ASTER) data. *Remote Sensing of Environment*, 84:350 – 366.
- Research Systems, Inc., 2002. ENVI Tutorials. Research Systems, Inc.,Boulder, CO, p. 640.
- Settle, J. J. (1996). On the relationship between spectral unmixing and subspace projection. *IEEE Transactions on Geoscience and Remote Sensing*, 34(4),1045–1046.
- Smith, M. O., Ustin, S. L., Adams, J. B., & Gillespie, A. R. (1990). Vegetation in deserts: 1. A regional measure of abundance from multispectral images. *Remote Sensing of Environment*, 31(1), 1–26.
- Settle, J. J., & Drake, N. A. (1993). Linear mixing and the estimation of ground cover proportions. *International Journal of Remote Sensing*, 14(6),1159–1177.
- Shimabukuro, Y. E., & Smith, J. A. (1991). The least-squares mixing models to generate fraction images derived from remote-sensing multispectral data. *IEEE Transactions on Geoscience and Remote Sensing*, 29(1), 16–20.
- Teillet, P.M., Guindon, B., Goodenough, D.G., 1982, On the Slope-Aspect Correction of Multispectral Scanner Data, *Canadian Journal of Remote Sensing*, 8, 84-106.
- Van der Meer, F., & De Jong, S. M. (2000). Improving the results of spectral unmixing of Landsat Thematic Mapper imagery by enhancing the orthogonality of end-members. *International Journal of Remote Sensing*,21(15), 2781–2797.
- Wu, C. (2004). Normalized spectral mixture analysis for monitoring urban composition using ETM+ imagery. *Remote Sensing of Environment*, 93(4),480–492.
- Xin Miao , Peng Gong, Sarah Swope, Ruiliang Pu, Raymond Carruthers, Gerald L. Anderson, Jill S. Heaton, C.R. Tracy ,(2006). Estimation of yellow starthistle abundance through CASI-2 hyperspectral imagery using linear spectral mixture models. *Remote Sensing of Environment* 101,329-341.
- Zeng XuBin, Robert E, Dickinson Alison Walker, et al. Derivation and evaluation of global 1-km fractional vegetation cover data for land modeling. *Journal of Applied Meteorology*; 2000. 39 (6):826-839.
-
- Foundation:** Major project of Fujian provincial department of science & technology. NO.2006F5029 and NO.2006F30104
- Author:** Wang Tianxing (1982-), M.Sc, specialized in inversion of land surface parameters ;Thermal infrared remote sensing, GIS application, Land Use and Land Cover Change. E-mail: watixi@163.com.TEL:13459194134
- mode, Stochastic Geometric model and Fuzzy model (Charles Lchoku,1996) to extract the sub-pixel information. Specially, the Linear Spectral Mixture Model(LSMM) is currently one of the most prevailing sub-pixel model for its simpleness and easily operation(Chabrilat, 2000),and has been broadly used in land-use and land-cover classification
- (Adams et al., 1995; Gong et al., 1994; Quarmby et al., 1992),land-cover change detection (Adams et al., 1995; Peterson & Stow, 2003), vegetation inversion(Patrick Hostert et al,2003), thermal feature extraction(Dengsheng Lu & Qihao Weng,2006) and geological surveys (Neville et al., 2003) during the past 30 years. Interestingly, some authors also found LSMM to be equivalent to the orthogonal subspace projection (OSP) method and linear support vector machine (SVM) (Brown et al., 2000; Settle, 1996).
- Linear Spectral Mixture Model also known as Linear spectral unmixing (LSU), sub-pixel sampling, or spectral mixture analysis(SMA), is a widely used procedure to determine the proportion of constituent materials within a pixel based on the materials spectral characteristics (Boardman, 1989),and followed by three assumption:(1) the spectra signals are linearly contributed by a finite number of land-cover classes (endmembers) within each pixel weighted by their cover percentage (Ichoku & Karnieli, 1996); (2) the endmembers in a pixel are homogeneous surfaces and spatially segregated without multiple scattering (Keshava & Mustard, 2002); and (3) the electromagnetic energy of neighboring pixels does not affect the spectral signal of the target pixel. Although nonlinear mixing effects due to the uncertainty caused by ,such as, atmospheric absorption and scattering, adjacent effect of pixel, have been considered in previous literature(Borel & Gerstl, 1994; Ju et al., 2003;Pu et al., 2003) they are complicated and case-specific and not seriously deteriorate the unmixing results(Xin Miao et al,2006;Chabrilat et al.,2000).
- Researches on LSMM in previous literature mostly focused on the evaluation of linear hypothesis relating to itself and techniques used to select endmembers and other uncertainties, nevertheless, the environment conditions of study area which could sway the unmixing-accuracy such as atmosphere reflectance or scattering and terrain undulation are not studied. The terrain effects are very notable from the satellite imagery

captured on undulating earth surfaces., These terrain illumination effects have serious consequences for the application of quantitative methods, including classification of land cover types and linear spectral analysis. So the main objective of this paper is to quantitatively evaluate the accuracy uncertainty of LSMM affected by the terrain undulation with the hope that this study could offer new theory basis for LSMM applications in mountainous area and furthermore improve the unmixing accuracy of LSMM. To this end, via taking unmixing vegetation abundance as an example, we choose the ASTER data equipped with relatively broad spectral range, fine spatial resolution, a large number of bands, and concentrated our study on part of suburb in Fuzhou, China. The following section is described to introduce the test site and the ASTER data followed by ASTER data processing. Then the C terrain undulation correction was used and subsequently LSMM was applied to both original ASTER data and C terrain undulation corrected ASTER image covering test site. Finally a regression analysis between vegetation abundances and NDVI, MVI extracted from originally or terrain corrected ASTER data using systematically sampling was implemented and the correlation coefficient as a indicator index was selected to quantitate the terrain undulate impact.

